Plasma sheet and (nonstorm) ring current formation from solar and polar wind sources

T. E. Moore,[1] M.-C. Fok,[1] M. O. Chandler,[2] C. R. Chappell,[3] S. P. Christon,[1] D. C. Delcourt,[4] J. Fedder,[5] M. Huddleston,[3] M. Liemohn,[6] W. K. Peterson,[7] and S. Slinker[8]

Received 27 April 2004; revised 7 October 2004; accepted 16 December 2004; published 19 February 2005.

[1] We consider the formation of the plasma sheet and geosynchronous region (nonstorm) ring current in the framework of collisionless test particle motions in three-dimensional magnetospheric fields obtained from self-consistent MHD simulations. Simulation results are compared with observations of the near-Earth plasma sheet from the Polar spacecraft during 2001 and 2002. Many particles were initiated in two regions representative of the solar wind source upstream of the bow shock and the polar wind source outside the plasmasphere, both of which are dominated by protons (H^+). Proton trajectories are run until they precipitate into the atmosphere, escape from the simulation space, or become stably trapped. These calculations produce a database of proton characteristics in each 1 R_E^3 volume element of the magnetosphere and yield velocity distributions as well as bulk plasma properties. We report results reflecting steady growth phase conditions after 45 min of southward interplanetary field, $B_Z = -5$ nT ($B_Y = 0$), and for conditions resulting after 2 hours of northward $B_Z = +5$ nT. The results for simulated velocity distributions are consistent with the Polar soundings of the current sheet from lobe to lobe and with AMPTE/CCE observations of (nonstorm) ring current region protons. The simulations help us identify the differentiation between solar and polar wind H^+ ions in observations. The weak NB_Z ring current-like pressure is primarily polar wind protons, while the moderately active SB_Z ring current-like pressure is primarily solar wind protons. The solar and polar wind contributions to the SB_Z ring current are comparable in density, but the solar protons have a higher average energy. For SB_Z, solar wind protons enter the nonstorm ring current region primarily via the dawn flank and to a lesser degree via the midnight plasma sheet. For NB_Z, solar wind protons enter the ring current-like region via the cusp and flanks. Polar wind protons enter the nonstorm ring current through the midnight plasma sheet in both cases. Solar and ionospheric plasmas thus take different transport paths to the geosynchronous (nonstorm) ring current region and may thus be expected to respond differently to substorm dynamics of the magnetotail.

Citation: Moore, T. E., et al. (2005), Plasma sheet and (nonstorm) ring current formation from solar and polar wind sources, *J. Geophys. Res.*, *110*, A02210, doi:10.1029/2004JA010563.

1. Introduction

[2] Since the definitive observation of geogenic (O^+) ions in the magnetosphere [*Shelley et al.*, 1972], it has been known that ionospheric cold plasmas contribute to the hot plasmas of the magnetosphere. However, it was also observed that heavy ions are important during times of magnetospheric storms, when there is substantial dissipation of energy in the ionosphere proper, below a few thousand kilometers altitude [*Peterson et al.*, 1981, 1982; *Sharp et al.*, 1985; *Hamilton et al.*, 1988; *Daglis et al.*, 1999]. Observations reveal that energy dissipated in the ionosphere goes partly into energization of heavy ions sufficient to overcome their gravitational binding to the Earth [*Sharp et al.*, 1977; *Freeman et al.*, 1977; *Klumpar*, 1979]. A review of the ionospheric supply of magnetospheric plasma sources is given by *Moore et al.* [1999]. More recent work by *Cully et al.* [2003] shows that the ionospheric supply of plasma to the plasma sheet, especially heavy O^+ plasma, is not only important but is

[1]NASA Goddard Space Flight Center, Greenbelt, Maryland, USA.
[2]National Space Science and Technology Center, NASA Marshall Space Flight Center, Huntsville, Alabama, USA.
[3]Vanderbilt University, Nashville, Tennessee, USA.
[4]Centre d'Etude des Environnements Terrestre et Planétaires, St. Maur, France.
[5]George Mason University, Vienna, Virginia, USA.
[6]University of Michigan, Ann Arbor, Michigan, USA.
[7]University of Colorado, Boulder, Colorado, USA.
[8]Naval Research Laboratory, Washington, D. C., USA.

0148-0227/05/2004JA010563$09.00

strongly modulated by convection as driven by the interplanetary magnetic field.

[3] The ionosphere has been known to supply cold light ion plasma to the magnetosphere since the discovery of the plasmasphere and the development of polar wind theory [*Banks and Holzer*, 1969; *Grebowsky*, 1970]. On openly convecting field lines, polar wind occurs continuously as convection opens the field lines and empties their accumulations into the polar lobes and downstream solar wind so that they never reach equilibrium pressures. Plasmaspheric plasmas result from polar wind-like light ion outflows into the nearly corotating inner magnetosphere, where they are trapped and accumulate to equilibrium pressures and are therefore called "refilling flows." Recently, the outer plasmasphere has been shown to flow sunward during magnetospheric disturbances [*Elphic et al.*, 1997; *Sandel et al.*, 2001; *Goldstein et al.*, 2002], and these cold plasmas have been discovered to be present in the subsolar low-latitude magnetopause region under a wide variety of conditions [*Su et al.*, 2001; *Chandler and Moore*, 2003; *Chen and Moore*, 2004]. When strong convection drains away part of the plasmasphere, the supply of plasma is enhanced in a transient way by the rapid release of accumulated plasma. Under steady conditions, however, the plasmasphere remains trapped and the magnetosphere is supplied only from the higher-latitude polar wind regions.

[4] The contribution of ionospheric light ions to magnetospheric hot plasmas is less well established and is complicated by the difficulty of discriminating protons of solar or geogenic origin. *Hill* [1974] estimated that polar wind was unlikely to contribute significantly to magnetospheric hot plasmas. *Christon et al.* [1994] used energy spectral features, in comparison with He^{++} assumed to be of solar origin, to estimate the relative contributions. They found that both solar wind and polar wind contributed comparable densities to the hot magnetospheric plasmas, with a somewhat higher ionospheric contribution for high solar activity levels but higher energies and pressures for the solar wind proton plasmas. The main motivation of this paper is to revisit the contribution of the polar wind plasmas to the plasma sheet and inner magnetospheric hot plasmas based on modern global simulations in comparison with observations.

[5] This paper is also motivated by observations of the layered structure of the plasma sheet boundary layer [*Eastman et al.*, 1984; *Parks et al.*, 1998] and a new data set from Polar/TIDE that reveals the lowest-energy extent of this structure in the ions that originate in the polar wind and auroral zones. We refer to these outflows through the lobes and into the plasma sheet boundary layer as "lobal winds," reflecting their pervasive presence throughout the magnetospheric lobes (M. W. Liemohn et al., Occurrence statistics of cold streaming ions in the near-Earth magnetotail: Survey of Polar-TIDE observations, manuscript in preparation for *Journal of Geophysical Research*, 2005), as well as the fact that in general they contain a mixture of light ion polar wind and heavy ion auroral outflows from the dayside and nightside.

[6] In this paper we simulate the light ion polar wind outflows that are pervasive, continuous, and at most weakly responsive to solar wind intensity or magnetospheric activity. We also simulate the entry of solar wind plasmas into the magnetosphere under the same conditions. We consider extreme conditions of purely southward and purely northward IMF, deferring consideration of more typical "Parker spiral" IMF with B_y dominant. We also defer consideration of auroral zone accelerated ionospheric outflows, including heavy ion outflows (predominantly but not exclusively O^+) associated with electromagnetic and kinetic energy dissipation within the ionosphere proper. The light ion auroral outflows have fluxes similar to polar wind, while the heavy ion outflows have fluxes that range from much less than to much greater than polar wind outflows depending on the free energy available [*Moore et al.*, 1999]. We address the question of how solar and polar wind protons are distributed in the magnetosphere at the extremes of interplanetary magnetic conditions and how their velocities are distributed at selected illustrative locations in the plasma sheet, its boundary layer, and in the inner magnetosphere. We consider quiet to active conditions when a modest nonstorm ring current exists in the geosynchronous orbit region. We do not consider the storm time ring current in this study.

2. Observations

[7] We begin by presenting relevant observations from the Polar spacecraft, the orbital apogee of which reached to the equatorial plasma sheet and swung through the midnight region during the fall of 2001 and 2002. The plasma sheet is highly dynamic on timescales that cannot be sampled continuously using the 18-hour orbit of Polar. However, during slow apogee passes through the plasma sheet, a dichotomy is observed between quiet periods when the current sheet is a few R_E thick (reversal of B_X) and active periods when the current sheet is much thinner with a thickness of only a few tenths of an R_E. During such active periods, individual or multiple substorm dipolarizations are observed, with associated strong plasma flow features. *Kletzing and Scudder* [1999] have previously reported on the characteristics of the electron plasma sheet, while TIMAS observations of the more energetic ion plasma sheet have been reported, e.g., by *Cattell et al.* [1999]. *Baker et al.* [2002] have reported a multispacecraft event study of substorm dipolarization events in the plasma sheet. *Nakamura et al.* [2002] explore the characteristics of near-Earth substorm events as observed in the plasma sheet. In the present paper, we focus instead on the steady structure of this region and the ion velocity distributions that define that structure in relatively quiet times, but we also point toward variations that would be expected in more active periods.

[8] Figure 1 illustrates typical characteristics of the plasma sheet as seen by the Polar TIDE investigation [*Moore et al.*, 1995], sampling energy from 0.3 eV to 450 eV, over the full range of spin angle around the orbit-normal spin axis of Polar. A pervasive feature of the magnetospheric lobe regions away from the current sheet is a cold "lobal wind." The term "lobal" is used here to apply to any high thermal Mach number plasma flows through the lobes, while "polar wind" is reserved for cold light ion outflows containing little if any O^+ outflows, which must originate from auroral processes and are therefore a subset of lobal winds. Thus lobal winds must originate in the high-latitude ionosphere

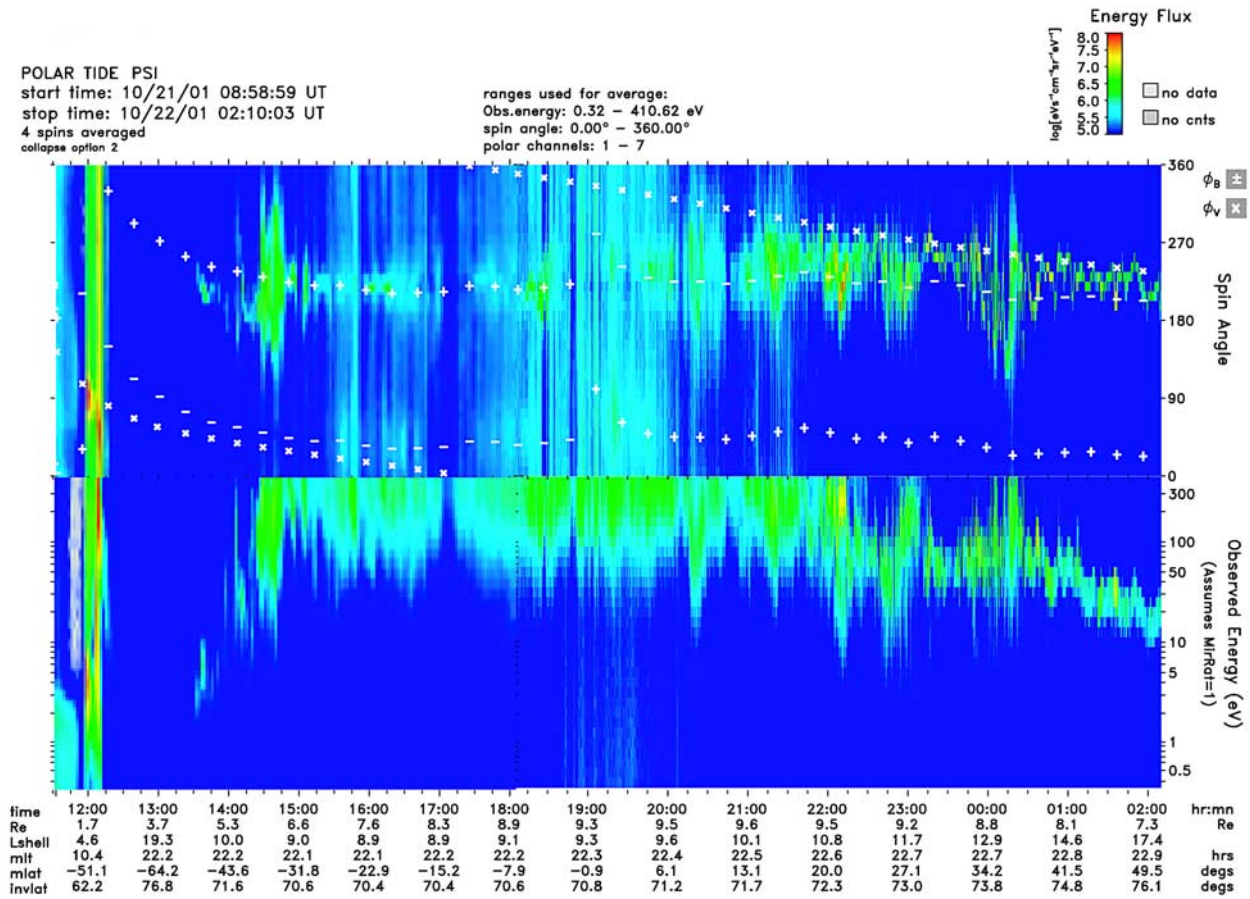

Figure 1. Polar/TIDE observations of the plasma sheet are plotted for an orbit on 21 October 2001, illustrating the following features: (a) lobal wind in both hemispheres, (b) bidirectional streaming in the plasma sheet boundary layer, (c) nearly isotropic warm plasma in the current sheet region, and (d) localized auroral acceleration and heating of the lobal wind outflows.

but may represent a mix of classical light ion polar wind and warmer components originating from the auroral zones or polar cap auroral features. These may contain a substantial or even dominant heavy ion component. Often, multiple species can be observed in the energy/charge distribution as multiple peaks [*Moore et al.*, 1997].

[9] Figure 1 also illustrates the typical formation of bidirectional streaming in the low-energy ions near but not at the magnetic current sheet. Such bidirectional streams are often asymmetric in temperature or Mach number, the beam traveling away from the plasma sheet being substantially warmer than the beam traveling toward the plasma sheet. Finally, Figure 1 illustrates the isotropization in angle and extension in energy beyond the TIDE range, which is typical in the plasma sheet near the current sheet. Figure 2 shows an example of the higher energy range ions and electrons associated with these current sheet crossings from the TIMAS and Hydra investigations. These have characteristic energies much higher than can be observed by TIDE but are limited to the regions near the current sheet.

[10] In addition to the features described above, a pervasive feature of the Polar observations in this region is a region of hot and therefore low Mach number flow of ions, embedded within the colder lobal wind outflows from the ionosphere. These are identified as nightside auroral zone ion outflows of either the beam or conic varieties. These appear with more or less prominence, presumably dependent upon the conjugate auroral activity on the flux tubes in which they appear. They are of higher parallel and perpendicular energy, with a broader angular pattern than the relatively cold lobal wind flows. While the range of energies is continuous, such auroral outflows are easily distinguished from the lobal wind flows within which they are usually embedded.

[11] In Figure 3, we summarize these observations schematically, showing the various velocity distribution types in their typical arrangement along a Polar orbit, relative to the current sheet, plasma sheet, and lobes. It can be seen that the plasma sheet appears as a layered structure of velocity distribution features, as described above. While there is considerable variability in the extent and prominence of the various features from pass to pass, presumably associated with substorm activity, a substantial repeatability of this pattern is observed over many passes through the region, and it can be considered to be an underlying structure upon which variations are superposed. In the following sections, we investigate the degree to which this structure can be

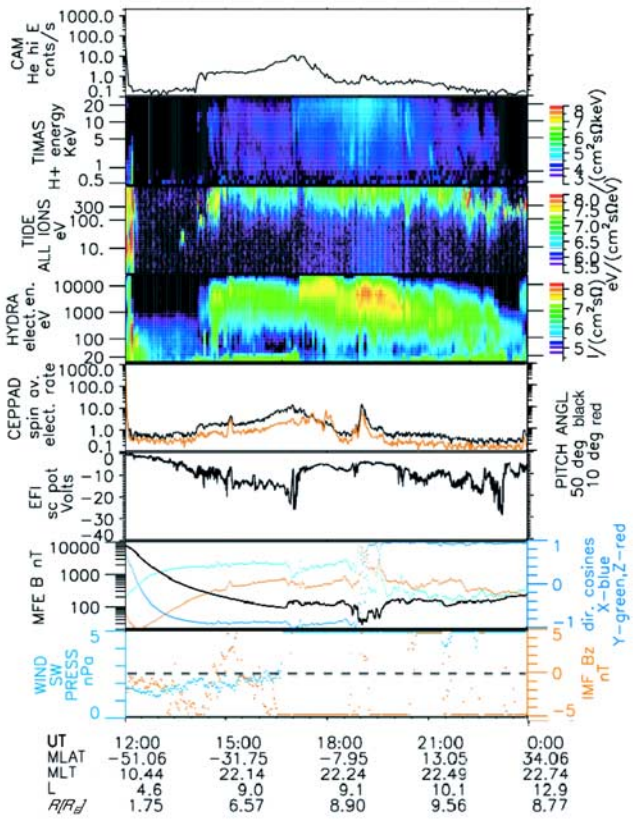

Figure 2. TIMAS and Hydra observations of hot plasma ions and electrons illustrating the full thermal extent of the hot isotropic current sheet plasmas.

understood in terms of the particle populations that enter and travel through the plasma sheet region.

3. Modeling

[12] For this study, M.-C. Fok adapted the full particle simulation of *Delcourt et al.* [1993] to use arbitrary fields specified on a grid. In the past, fields have been specified by empirical models that can be evaluated continuously at any point in space. However, in the present calculation, these empirical model fields are replaced by the self-consistently computed fields from the magnetohydrodynamic (MHD) simulation of Lyon, Fedder, and Mobarry [*Fedder et al.*, 1995; *Mobarry et al.*, 1996; *Slinker et al.*, 1998; *Slinker et al.*, 2001]. The LFM grid is a nonuniform, distorted spherical grid with polar axis aligned to the SM-X axis. The grid extends roughly 24 R_E sunward to $X = -300$ R_E tailward and 90 R_E in the Y and Z directions. The grid has 50 cells in the radial direction, 50 cells in the polar direction, and 64 cells in the azimuthal direction. The spacing in azimuthal angle is uniform. The grid spacing in polar angle and radius vary, with higher resolution on the dayside and in the near-Earth region. The interior of the grid is a spherical region with a radius of 3.2 R_E centered on the Earth.

[13] The spatial resolution of this grid is well visualized by *Slinker et al.* [2001]. In the spherical shell for the inner boundary at $r = 3.2$ R_E to $r = 10$ R_E there are approximately 49,000 grid points with an average volume per cell of 0.08 R_E^3. For the shell out to $r = 15$ R_E, approximately 77,000 points with average cell volume of 0.18 R_E^3 and for the shell out to $r = 20$ R_E, 90,000 grid points with volume about 0.35 R_E^3. Also relevant here is the box volume from -25 to 15 in x_{GSM} and -20 to 20 for y and z. This volume of $40 \times 40 \times 40 = 64{,}000$ R_E^3 has about 103,000 grid points with an average cell volume of 0.6.

[14] For computational efficiency, we resampled the LFM fields onto a spherical grid with polar axis aligned to the GSM X axis. The spacing in polar angle is a uniform 2° and the resolution in azimuthal angle on the GSM XY plane is ~5.5°. The grid spacing in radius varies with polar and azimuth angles at higher spatial resolution on the dayside and lower on the nightside. This approach allows very rapid identification of the current cell in which a particle is positioned as it moves.

[15] Integrating particle trajectories requires a method for interpolating between the grid points of the MHD simulation to enable calculation of field values at any point, as a particle moves about within the simulation space. A number of technical issues arise in performing this interpolation. For example, it can be shown that a simple linear interpolation in three dimensions is the only procedure that preserves the divergence free requirement on the magnetic field components. Therefore we use here a simple linear interpolation in place of more sophisticated techniques that would allow continuous field gradients at the grid points. The inevitable field gradient discontinuities at grid points are a source of numerical diffusion, increasing with the coarseness of the grid used.

[16] For time stepping, our approach is to step the particles a large number of times per gyro period, typically 72 times or every 5° of gyrophase, using Delcourt's double precision implementation of a fourth-order Runge-Kutta algorithm. This is more accurate than required for the trajectory durations we use. We have previously shown [*Moore et al.*, 2000] that the trajectories are precisely reversible over flight paths of many tens of R_E and many hours.

[17] To test the performance of the finite element interpolation approach used here, we resampled the analytically continuous (T98-Stern-Volland) field models onto our magnetohydrodynamic field grid and compared typical trajectories with the same initial conditions. We found that the results were indeed sensitive to grid spacing, indicating numerical errors. To minimize such effects, we used the finest practical grid spacing for our MHD simulation fields and determined that the numerical effects were substantially reduced. The main effect of such errors is a diffusive effect on the particle trajectories.

[18] For the solar wind, initial positions were randomly selected from a uniform distribution over a GSM yz plane at $x = 15$ R_E, upstream of the simulated bow shock. For the polar wind, we started protons at 4 R_E altitude with invariant latitudes uniformly distributed above 55° and over all local times. Auroral acceleration processes have not been applied to polar wind originating in that region, but the total escaping flux of protons is relatively unaffected by such processes [*Moore et al.*, 2000]. Initial velocities were selected randomly from a uniform distribution of width equal to the specified thermal speed, as shown in Table 1. Particles were run until they precipitate into the atmosphere,

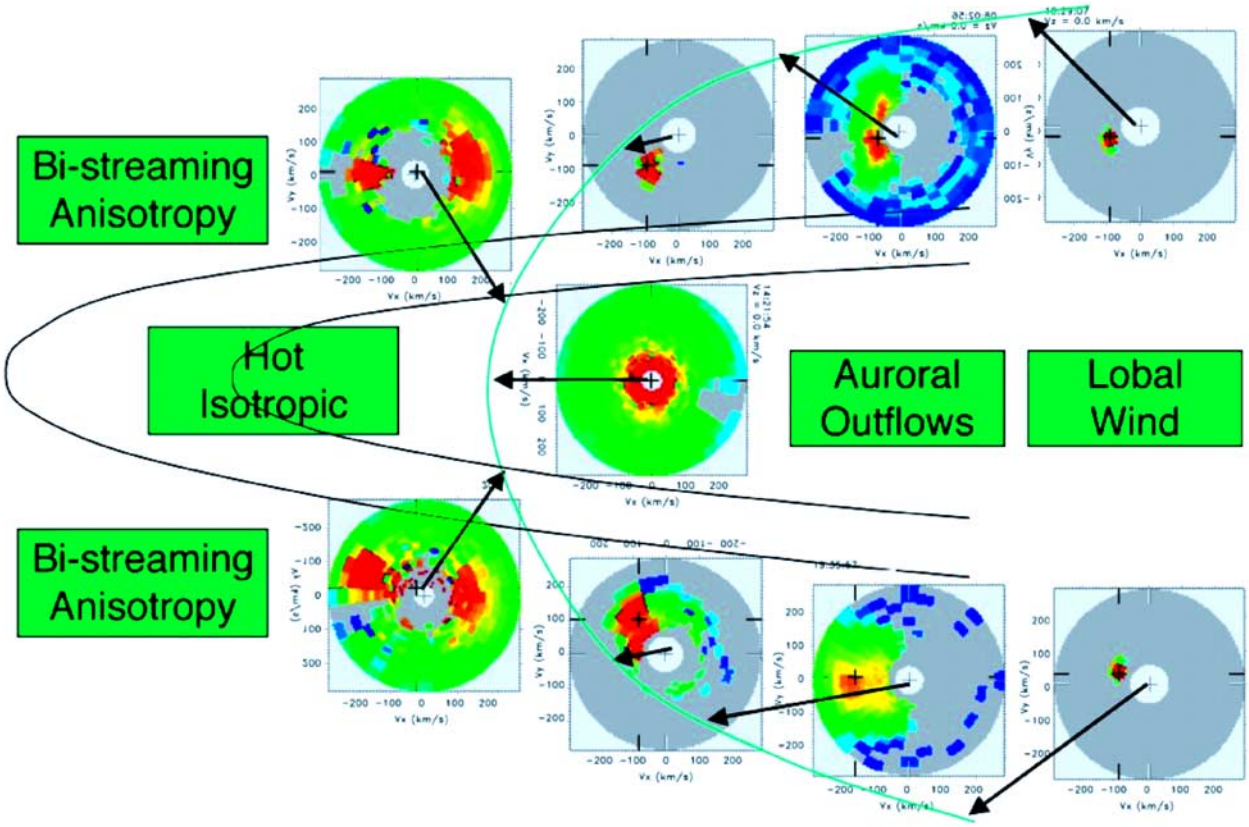

Figure 3. A schematic collage of the various velocity distribution types and their association with observing position relative to the current sheet along a typical polar orbit.

escape from the simulation volume, or exceed a time limit up to 24 hours, sufficient for cold particles to corotate once around the Earth.

[19] A large number of particle trajectories was run and accumulated into a spatial database of bins with resolution of 1 R_E^3 for both solar wind and polar wind particles. The record for each particle consists of one line describing the particle initial conditions and many lines describing the particle state as it crosses each boundary in physical space. In general, particles were run with randomly selected initial velocities (within specified ranges) until the regions of greatest interest contained of order 100 particles per bin. Some bins tend to remain empty, particularly for solar particles, because most of them pass through the system without entering the magnetosphere. To counter this, additional solar particles were run, focusing on the upstream regions with high probability of entry, until the primary solar wind entry path and inner magnetosphere bins contained >100 solar particles. Requiring 100 particles in each bin provides minimal statistics for the estimation of bulk properties of the plasma at the 10% accuracy level and crude particle velocity distributions along the primary transport paths for the particles.

[20] Bulk properties were estimated following an extension of the method described by *Chappell et al.* [1987] and *Delcourt et al.* [1989]. Examples of both are exhibited in subsequent figures. For each particle in a given spatial bin, the particle velocity and transit time for that bin are calculated. For a particle (i) passing through a particular bin (j), the contribution of density in this bin by this particle is

$$n_{ij} = F_i \times T_{ij}/V_j, \tag{1}$$

where F_i is the ion source flux in ion/s for particles of the specified velocity, T_{ij} is the residence time of particle i in bin j, and V_j is the volume of bin j, that is 1 R_E^3 in our case.

[21] F_i is computed directly from the density and flow of the source plasma across the source boundary.

$$F_i = n_s \times v_s \times dA;\ dA = A/N_T. \tag{2}$$

Here dA is the area of the source surface allocated to each particle, which is the total area of the source divided by the

Table 1. Source Region Particle Initial Conditions

Parameter	Value	Comment
	Solar Wind	
Density	6.5 cm^{-3}	typical
Thermal speed (temp)	31 km/s (kT = 5 eV)	"
Velocity	400 km/s	"
Mean PSD	2×10^{11}	
	Polar Wind	
Density	0.5 cm^{-3}	[*Su et al.*, 1998]
Thermal speed (temp)	17 km/s (1.5 eV)	"
Velocity	100 km/s	"
Mean PSD	2×10^{11}	"

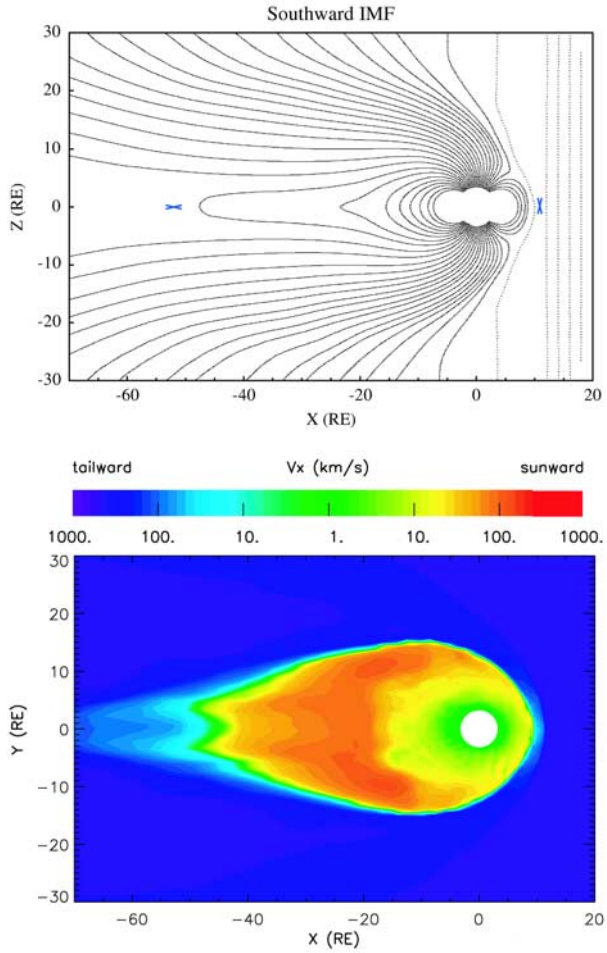

Figure 4. The computed magnetohydrodynamic fields for the SB_Z case. (top) The magnetic (B) lines are indicated in the noon-midnight meridian. (bottom) The electric field is indicated as color contoured values of the Vx in the GSM-XY plane, coded to discriminate sunward (reddish) from tailward (bluish) flows, with green indicating regions of relatively low-velocity flows.

number of particles emitted, assuming a uniform distribution of particle emission on the source surface, which is must be assured when randomizing the initial locations. The source number density and flow velocity may be specified, or the product of those two is just as useful, if better known.

[22] Substituting (2) into (1), we have

$$n_{ij} = n_s \times v_s \times A \times T_{ij} / \left(V_j \times N_T\right). \tag{3}$$

The density at bin j is just the summation of n_{ij} over all particles that are passing through bin j:

$$n_j = \text{Summation in } i \ \left(n_{ij}\right). \tag{4}$$

These relations can be applied to any source flowing across a boundary surface. The density from the ionospheric outflow can be calculated in a similar way. In that case, V_{SW} should by replaced by V_{PW} and other parameters are replaced with values appropriate to the polar wind.

[23] Once densities are calculated, pressure at bin j is given by

$$P_j = \text{Summation in } i \ \left(P_{ij}\right)$$

$$P_{ij} = n_{ij} \times E_{ij},$$

where E_{ij} is the average energy of particle i in bin j.

[24] For the solar wind case, $n_s = 6.5$ cm^{-3}; $v_s = 400$ km/s or 4e7 cm/s; $A = 3600$ R$_E^2$; $N_T = 2{,}600{,}000$. Total solar wind proton fluence through the simulation is 2.9×10^{35} ion/s. For the polar wind case $n_s \times v_s = 7.1\text{e}6$ cm^{-2}s^{-1} (3e8 at 1000 km); A = area of sphere 4 R$_E$ radius for invariant latitudes above 55° = 18.18 R$_E^2$; $N_T = 20{,}000$. Total polar wind proton fluence through simulation is 1.05×10^{26} ion/s.

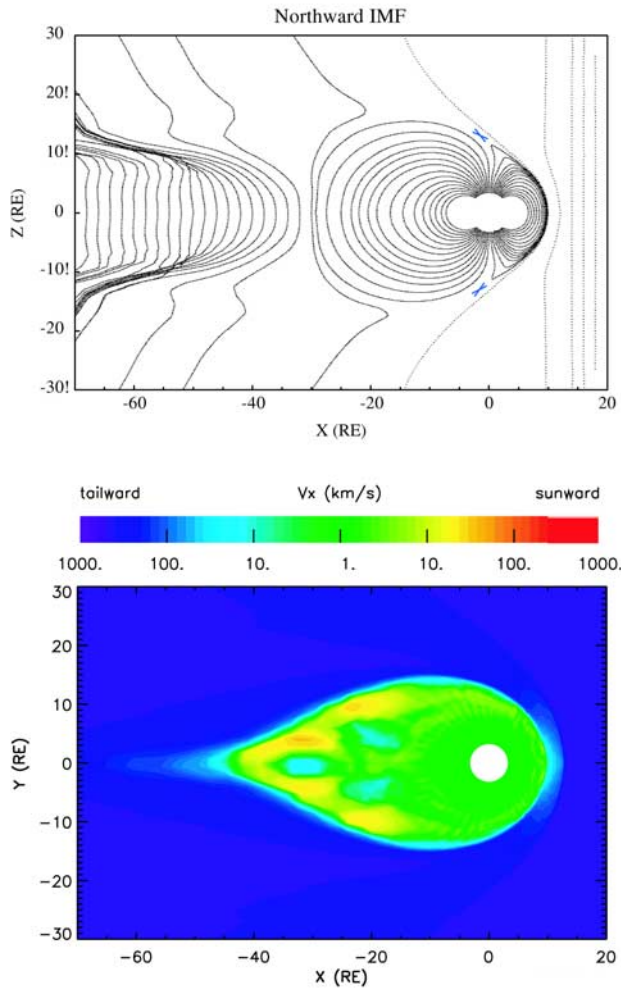

Figure 5. The computed magnetohydrodynamic fields for the NB_Z case. (top) The magnetic (B) lines are indicated in the noon-midnight meridian. (bottom) The electric field is indicated as color contoured values of the Vx in the GSM-XY plane, coded to discriminate sunward (reddish) from tailward (bluish) flows, with green indicating regions of relatively low-velocity flows.

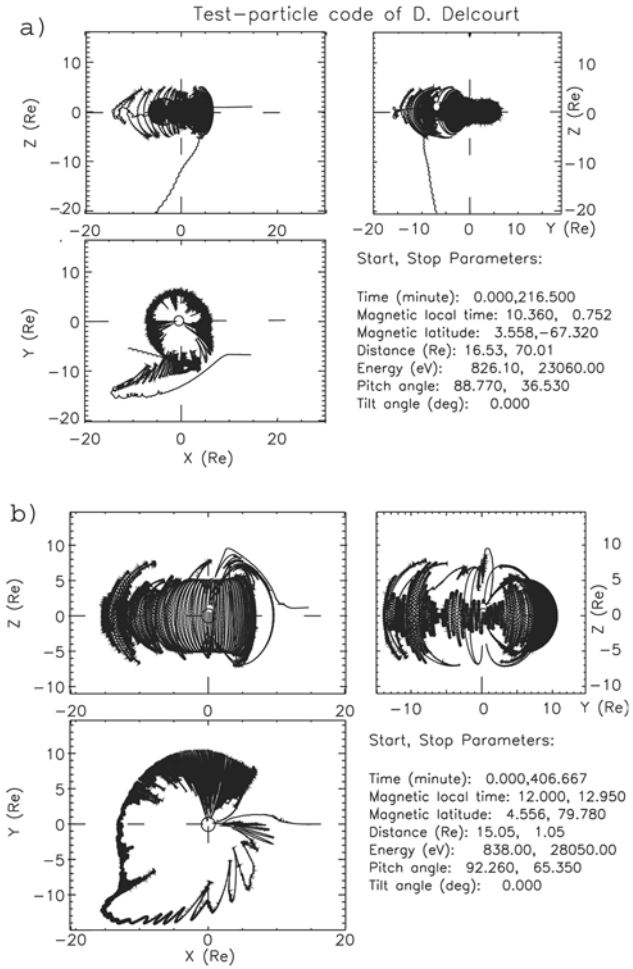

Figure 6. Example trajectories for solar wind entry in (a) the SB_Z case and (b) the NB_Z case. Insets in each panel show the *YZ* plane projection as seen from the Sun.

[25] For the polar wind case, this total is based on local fluxes rather than total fluence, and the local fluxes have been taken to be as high as credible. In practice, nightside fluxes would be somewhat smaller than we have used here, by a factor as small as 0.1 (factor <2 in total fluence).

[26] This method of computing bulk properties allows for the diffusive filling of velocity space from source populations that tend to be highly structured in velocity space at any particular location [*Moore et al.*, 2000]. If the fields we use were realistic on all spatiotemporal scales and there were no diffusive processes present, observed velocity distributions would be very finely structured with narrow features. In practice, magnetospheric fields include fluctuations over a wide range of frequencies, which are evidently diffusive, since extremely fine features are not observed within hot plasmas, though of course certain anisotropies are observed, as discussed above. Our bulk properties calculation attributes to each particle both a mean phase space density and a velocity space volume over which each particle is representative of the source. Thus the units of our particle weightings are [cm^{-3}], per equation (4) above.

[27] In Figures 4 and 5, we display plots of the MHD fields, as they are specified at two points in time by the LFM MHD simulations. The simulation is for a time sequence that involves a few hours of northward B_z, an abrupt southward turning for 2 hours, and finally, a return to northward IMF [*Slinker et al.*, 1995]. For the NB_Z case of this study, we selected a time 2 hours after the establishment of northward IMF, to allow stabilization under those conditions. For the SB_Z case, we selected a time about 45 min after the southward turning, well after the formation of a distant reconnection *X* line but well before the appearance of a near-Earth *X* line and ejection of a plasmoid. That is, we chose a state representative of the substorm growth phase, when the magnetotail closely resembles a Level −2 T89 field (corresponding to $Kp \sim 1-2$) earthward of the distant neutral line at ∼40 R_E. This choice for the MHD field snapshot was motivated by a desire to maintain rough consistency with earlier simulations that have been done in the Stern-Volland-T89 field models [*Stern*, 1975; *Volland*, 1978; *Tsyganenko*, 1989] and with Polar observations of the quiet inner plasma sheet, which are best fit by a T89 activity level of 2 out of 6. For such cases, the current sheet as sampled by Polar is moderately thick, rather than being a thin sheet case typical of strong activity. The inner magnetosphere at this time contains stably trapped circulating ions in the geosynchronous orbit region that we refer to as "nonstorm ring current" because this is not representative of a storm time ring current.

[28] For the SB_Z case of Figure 4, subsolar reconnection and distant plasma sheet reconnection are indicated by the blue "x" markings in the figure. Subsolar reconnection drives a high-latitude flow that reinforces and becomes part of the double cell circulation flow in the equatorial plane, as shown in the lower panel of the figure. The magnetotail pressure distribution drives an earthward flow up to about 150 km/s in the inner plasma sheet. The action of the distant neutral line helps to inflate the plasma sheet during this period but is being convected tailward and has little influence on driving sunward convection at this point in the growth phase. The transpolar potential for this case is 130 kV.

[29] For the NB_Z case of Figure 5, there is high-latitude reconnection above the cusps, again indicated by the blue "x" markings in the figure. Reconnection is peeling off magnetotail plasma flux tubes and shedding them downstream. The convection flow pattern for the NB_Z case shows a complex transient system of eddy flows in the plasma sheet, parts of which feed the high-latitude shedding of plasma. In addition, a much weaker double cell pattern is present in the inner magnetosphere. The transpolar potential for this case is only 13.6 kV.

4. Results

4.1. Fluid Bulk Parameters

[30] Trajectories typical of polar wind outflow have been previously published, e.g. by *Delcourt et al.* [1993, 1994], and are not much affected by the use of MHD fields, though the quantitative details may vary owing the detailed differences in the fields. The advantage of using MHD fields is that we can now consider the entry of solar wind through realistic boundary layer fields with reconnection operative. This allows us to more realistically assess solar wind entry, than was the case in the work of *Delcourt et al.* [1992], where we had to introduce solar wind particles inside the

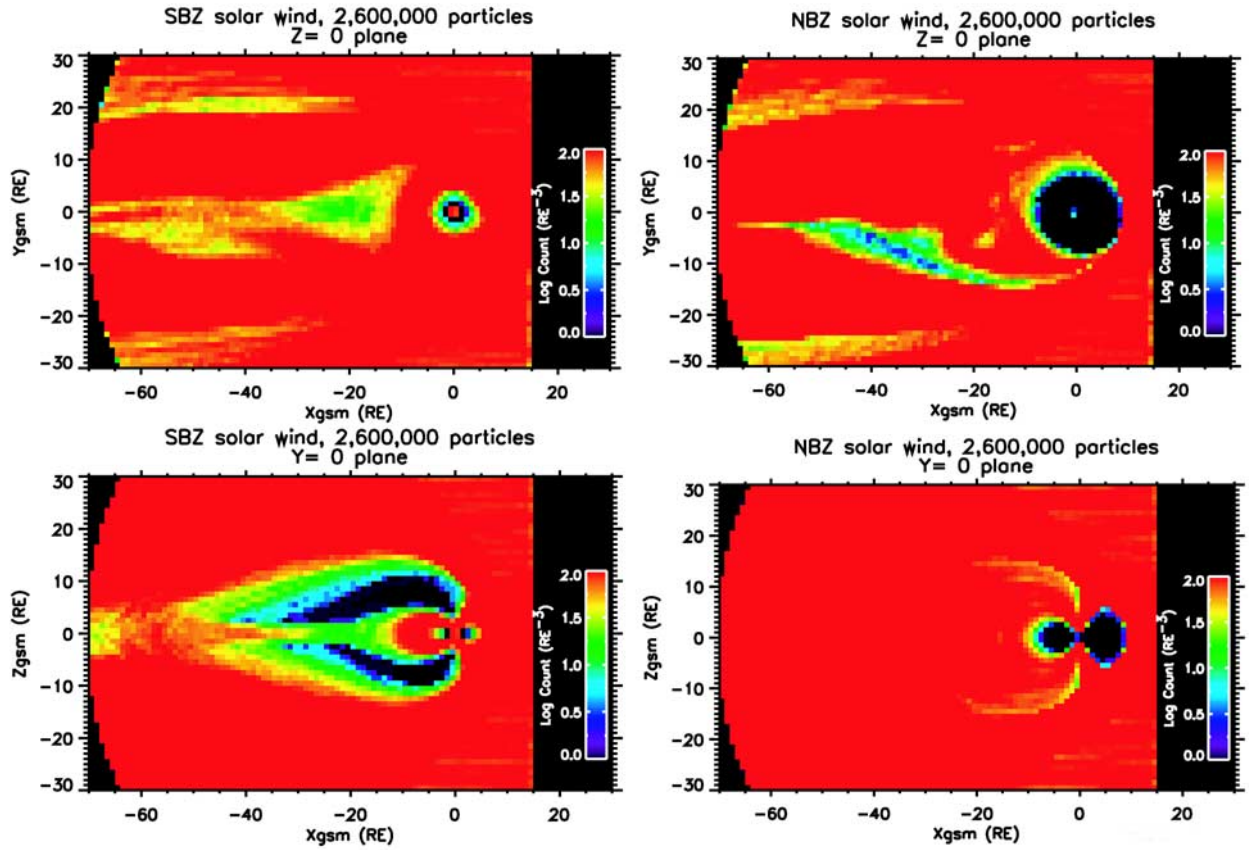

Figure 7. The distribution of particles within the simulation space for SB_Z. (left) Solar wind proton counts per bin for (top) *XY* and (bottom) *XZ* planes. (right) The same distributions for polar wind protons. The scale saturates at 100 particles per bin.

magnetopause or cusp and could not readily explore the low-latitude boundary layer (LLBL) as an entry region.

[31] Figure 6 shows examples for solar wind entry in southward and northward cases in Figures 6a and 6b, respectively. These trajectories were typical among those selected with the criterion that they begin in the solar wind and subsequently enter a box of dimension ± 6 R_E, centered on Earth, that is, near or inside geosynchronous orbit. These ions gain substantial energies and become part of the nonstorm ring current distribution. In Figure 6a the proton begins by going along the dawn flank but then slows and turns around at $x \sim -16$ R_E and travels back toward the Earth on the dawnside, entering into a conventional bouncing and drifting trajectory as it gains energy to the 28 keV range from the convection electric field.

[32] In Figure 6b for the NB_Z case, entry is via the dayside cusp, where the proton penetrates quite deeply, and subsequently enters into the LLBL flow, but on the inside of the magnetopause on closed flux tubes where it bounces up and down substantially in Z_{GSM}. It eventually enters a trajectory that resembles the SB_Z case but at substantially larger radius from the Earth and with slightly lower energy in the 23 keV range.

[33] To further establish the nature of the particle trajectories and statistics within bins, we next exhibit a plot of the distribution of particles within the simulation space in Figure 7. In the inner magnetosphere and much of the plasma sheet, we approach or exceed 100 particles without collapsing bins.

[34] In Figure 8 we display, for the SB_Z case, the plasma pressure in the GSM-XZ or noon-midnight meridian plane. Here the bow shock and magnetosheath are prominent features, as are the cusps and the cross section of the ring current-like region. Solar wind protons form north and south mantles with outward pressure gradients from the cores of the lobes. Here the velocity filtering effect is spreading the solar protons out with the slowest ones convected most deeply toward the current sheet and reaching it in appreciable quantities at $30-40$ R_E with some asymmetry.

[35] In the polar wind case, the polar outflow by definition fills the lobes and has properties in good agreement with Polar observations of the high-altitude polar wind [*Su et al.*, 1998]. Much of the polar wind reaches the plasma sheet earthward of about -40 R_E and convects back toward the Earth to form a region of drifting ring current-like protons. Polar wind protons also convect to the magnetopause where they are jetted up over the poles, participating in the magnetosheath and mantle flow as they escape downstream.

[36] In Figure 9, we display, for the SB_Z case, the plasma pressure in the XY or equatorial plane. The solar wind case again illustrates the bow shock and the magnetosheath, the low-latitude boundary layer flows, and formation of a cavity

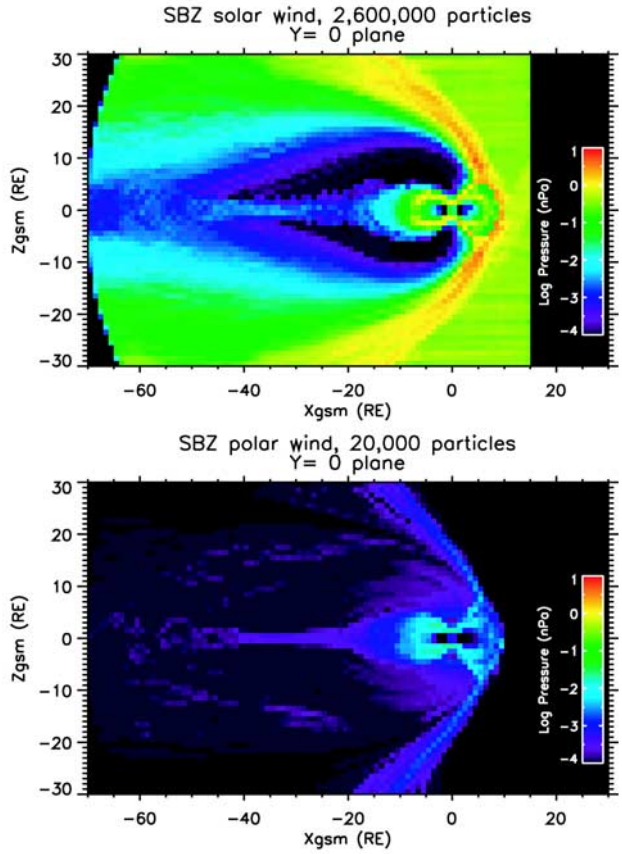

Figure 8. For the SB_Z case, the plasma pressure is color-contoured in the GSM-*XZ* or noon-midnight meridian plane. (top) Solar wind particle pressures and (bottom) polar wind particle pressures.

in the wake region, within which there is a much lower pressure than in the solar wind proper or the magnetosheath. Low-latitude boundary layers on both flanks have pressures approaching the upstream solar wind pressure. The dawn flank trajectories illustrated in Figure 6 can be seen as a return flow on the dawn flank into the circular drifting ring current-like population, with a pressure reaching $\sim$1 nPa. This feature is not as close to Earth as a full storm-time ring current, reflecting weak inner magnetospheric convection. This owes in part to the moderate SB_Z conditions for this simulation and in part to inherent limitations of MHD simulations of the inner magnetosphere.

[37] Polar wind ions populate the plasma sheet, escaping downstream where they land beyond the convection reversal of Figure 5 and returning earthward where they land within the earthward flow. The latter illuminate a clear plasma sheet structure that connects directly with the inner magnetospheric closed drift region, having pressure comparable to that of the solar wind protons in that same part of the plasma sheet. Polar wind plasma that is convected to the sunward reconnection region is forcefully launched into the magnetosheath flows along the low-latitude flanks of the magnetosphere and downstream with the solar wind boundary layer flow.

[38] In Figure 10, we display for the SB_Z case the proton pressure in the last of the three cardinal planes, the GSM-YZ plane at $X = 0$. This cross section again shows solar wind and magnetosheath flows and now shows the cross section of the lobes, which are visible in both solar wind and polar wind proton pressure, though for solar protons, their centers are profoundly empty, having pressures even lower than that of the polar wind outflows, as observed by Polar [*Su et al.*, 1998]. The magnetosheath contains an enhancement of polar wind proton pressure, but it remains a minor contribution to the solar wind pressure there. The cross section is also suggestive of the solar wind entry via the flanks that is visible in Figures 6 and 9.

[39] We next switch to the NB_Z case and display the plasma pressure in the *XZ* or noon-midnight meridian plane in Figure 11. The solar wind tail cavity still remains but is not as low in pressure, particularly in the polar lobes. Without lobes, the plasma sheet is hardly recognizable and is distributed all the way up into the polar caps, where it nearly meets a cusp that extends farther antisunward than in the SB_Z case. Sunward convection of plasma sheet material results from the action of high-latitude reconnection above the cusps drawing the magnetotail plasmas into the lobes and polar cap, where plasma tubes are peeled off by high-latitude reconnection. Note that this case has the $B_Y = 0$ with perfectly northward IMF.

[40] The polar wind outflows for NB_Z similarly show no narrow plasma sheet feature. Escape occurs onto recon-

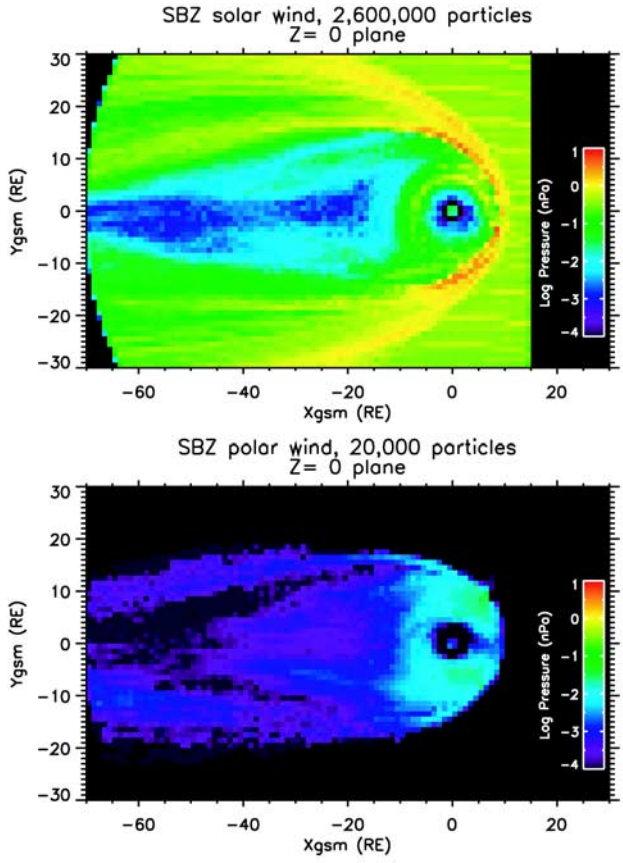

Figure 9. For the SB_Z case, the plasma pressure is color-contoured in the GSM-*XY* or equatorial plane. (top) Solar wind particle pressures and (bottom) polar wind particle pressures.

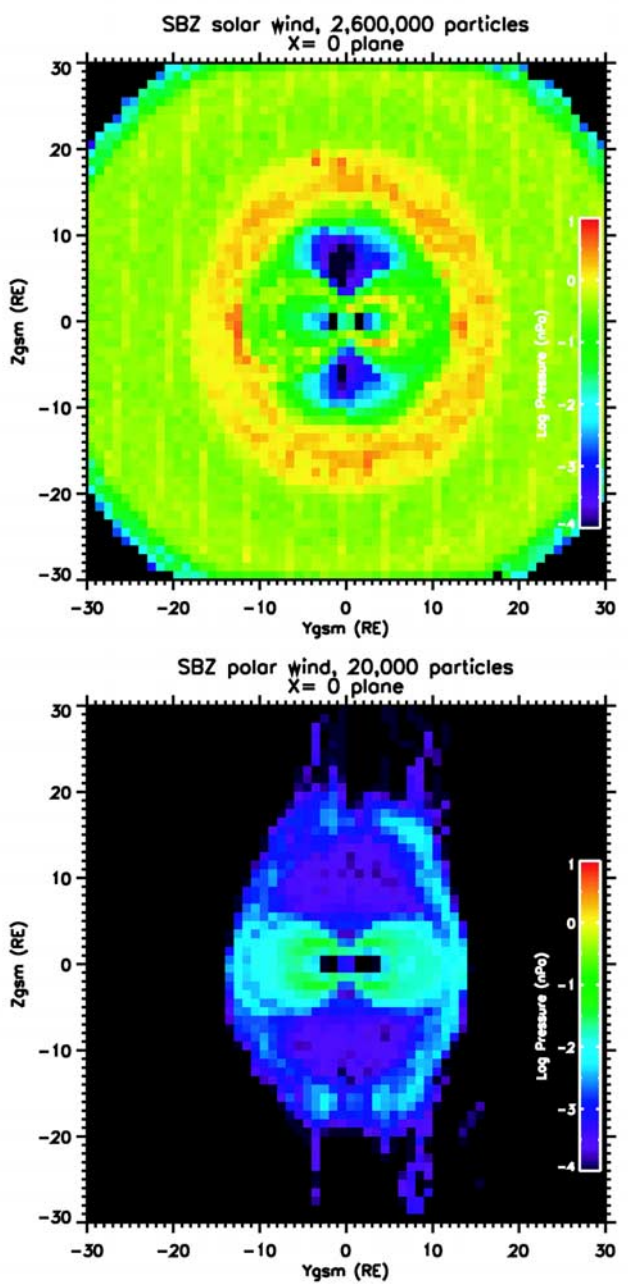

Figure 10. For the SB_Z case, the plasma pressure is color contoured in the GSM-*YZ* or dawn-dusk meridian plane. (top) Solar wind particle pressures and (bottom) polar wind particle pressures.

nected flux tubes shed downstream at high latitudes. The prominent magnetosheath jets of polar wind ions seen in the SB_Z case are much weaker in this NB_Z case.

[41] In Figure 12, the pressure in the *XY* or equatorial plane is shown for NB_Z. For solar protons, it can be seen that the tail cavity of exclusion is considerably shorter and weaker than was the case for SB_Z and contains some complex features reflecting the vortices in the fields. Dawn and dusk LLBLs exist but flow tailward into the plasma sheet, forming a cold dense plasma sheet. We know from looking at individual trajectories that entry into the innermost region begins in the cusp and passes through the LLBLs for NB_Z. The entry "plume" appears to extend into the plasma sheet diagonally in this case, rather than going mostly to the closed ring current-like region as it did for SB_Z. Apparently, as a result, the ring current that forms is much more modest in pressure at ~0.01 nPa and farther from Earth than for SB_Z. This result indicates a modest solar contribution to the quiet NB_Z ring current.

[42] The polar wind for NB_Z also has about the same pressure in the ring current-like region as for SB_Z ($\sim 3 \times 10^{-2}$ nPa), but the pressure peaks farther from Earth than for SB_Z. Nevertheless, the polar wind protons extend closer to the Earth and are comparable in pressure content to the solar protons in the ring current-like region for this case.

[43] Figure 13 displays the corresponding NB_Z results for pressure in the YZ plane or dawn-dusk meridian. This plot complements the other cuts and shows that the plasma sheet like extension over the poles, meeting the cusps, is indeed localized in the noon-midnight meridian plane, forming a feature reminiscent of a theta aurora. Simulations with finite B_Y would likely shift this feature across the polar cap as the high-latitude convection varies in response.

[44] The polar wind pressure distribution in this plane shows a ring current-like feature. Owing to the very weak

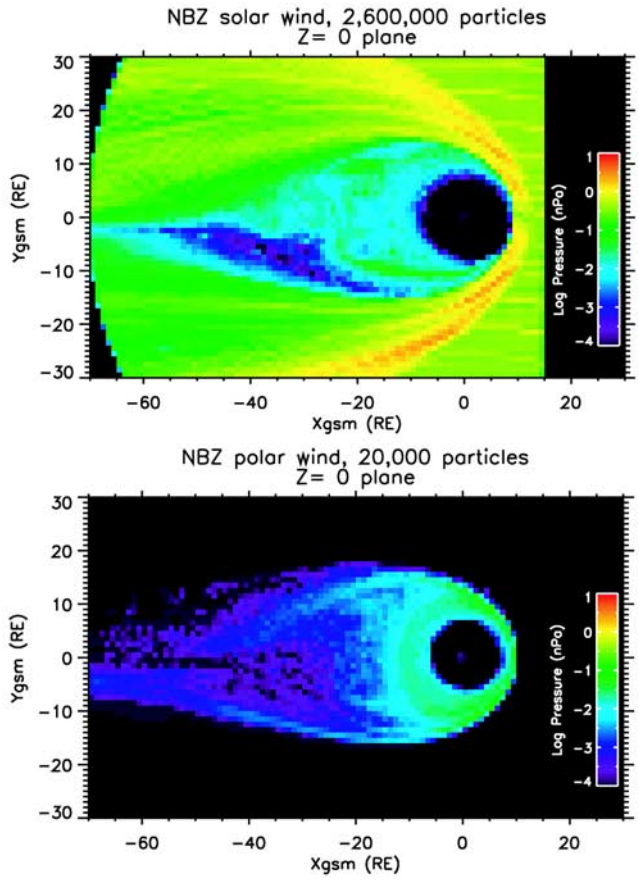

Figure 11. For the NB_Z case, the plasma pressure is color contoured in the GSM-XY or equatorial plane. (top) Solar wind particle pressures and (bottom) polar wind particle pressures.

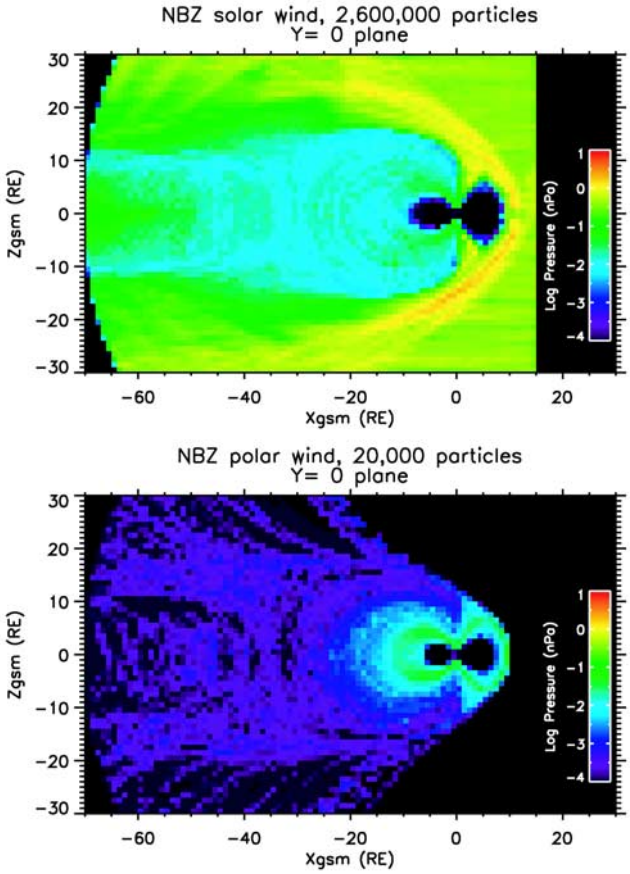

Figure 12. For the NB_Z case, the plasma pressure is color contoured in the GSM-XY or equatorial plane. (top) Solar wind particle pressures and (bottom) polar wind particle pressures.

inner magnetosphere plasma flows, this feature forms outside 5–6 R_E. There is little if any magnetosheath flow of polar wind protons, presumably because this plasma is being stripped off the polar regions by high-latitude reconnection, instead of returning to the subsolar region and escaping into the magnetosheath upstream of $X = 0$.

4.2. Kinetic Properties

[45] We now examine particle velocity distributions for the SB_Z case in Figure 14, showing solar wind protons on the left and polar wind protons on the right, at $X = -9.5$, $Y = 0.5$ R_E, and for Z ranging from north lobe to south lobe. This location provides a good comparison with the data presented earlier from Polar/TIDE, obtained from a similar location of about 9.5 R_E at apogee.

[46] In the right-hand or polar wind column of Figure 14, we find a cold low-energy beam of polar wind protons traveling tailward along the magnetic field in both lobes, as expected, toward the current sheet. As we move closer to the current sheet from either lobe, a heated population appears, streaming opposite to the cold tailward flow, traveling away from the current sheet and toward Earth. This is the cold polar stream from the opposite hemisphere after passing through the sharply curved, convecting neutral sheet where they have been energized and spread in pitch angle by differences in their arrival gyrophase. Moving closer to the current sheet, the local cold beam begins to get warmer in response to the increasing field curvature, becoming similar to the hot counterstreaming population that is traveling away from the current sheet, producing a warm isotropic population, resulting from current sheet accelerations. In addition there is an apparent hotter population of polar wind protons, extending to 50 keV or so just at the current sheet. We find that these hot polar wind protons have never traveled beyond ~15 R_E from Earth prior to arrival at this location and thus are polar wind

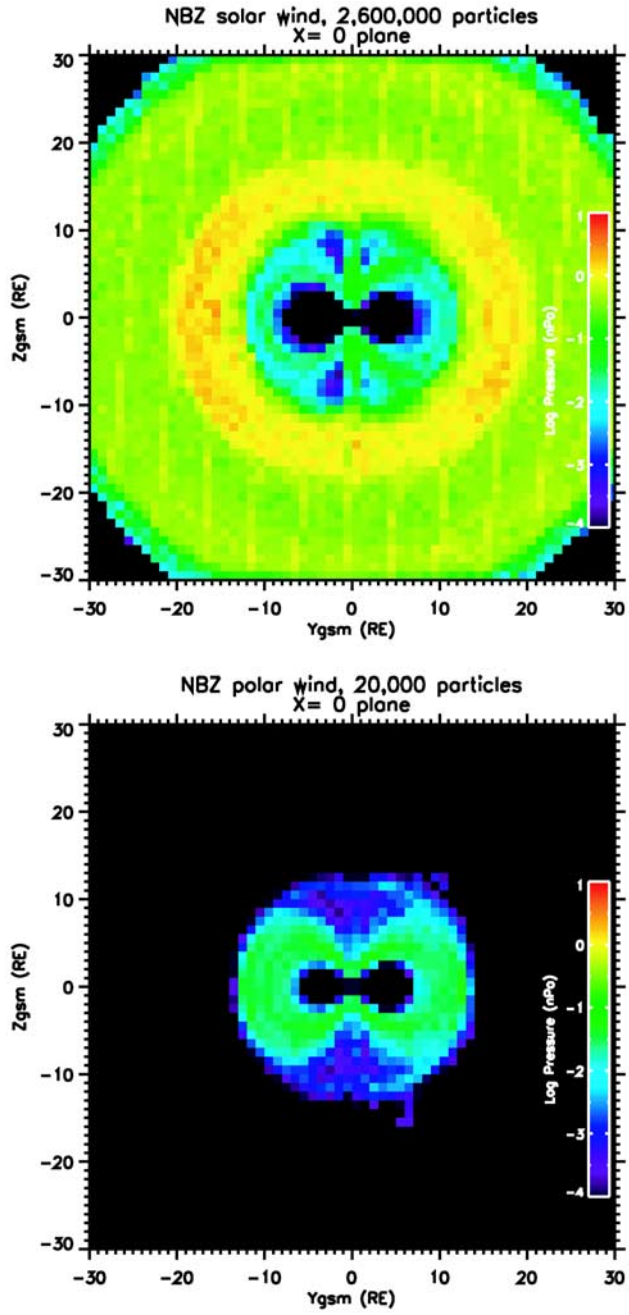

Figure 13. For the NB_Z case, the plasma pressure is color contoured in the GSM-YZ or dawn-dusk meridian plane. (top) Solar wind particle pressures and (bottom) polar wind particle pressures.

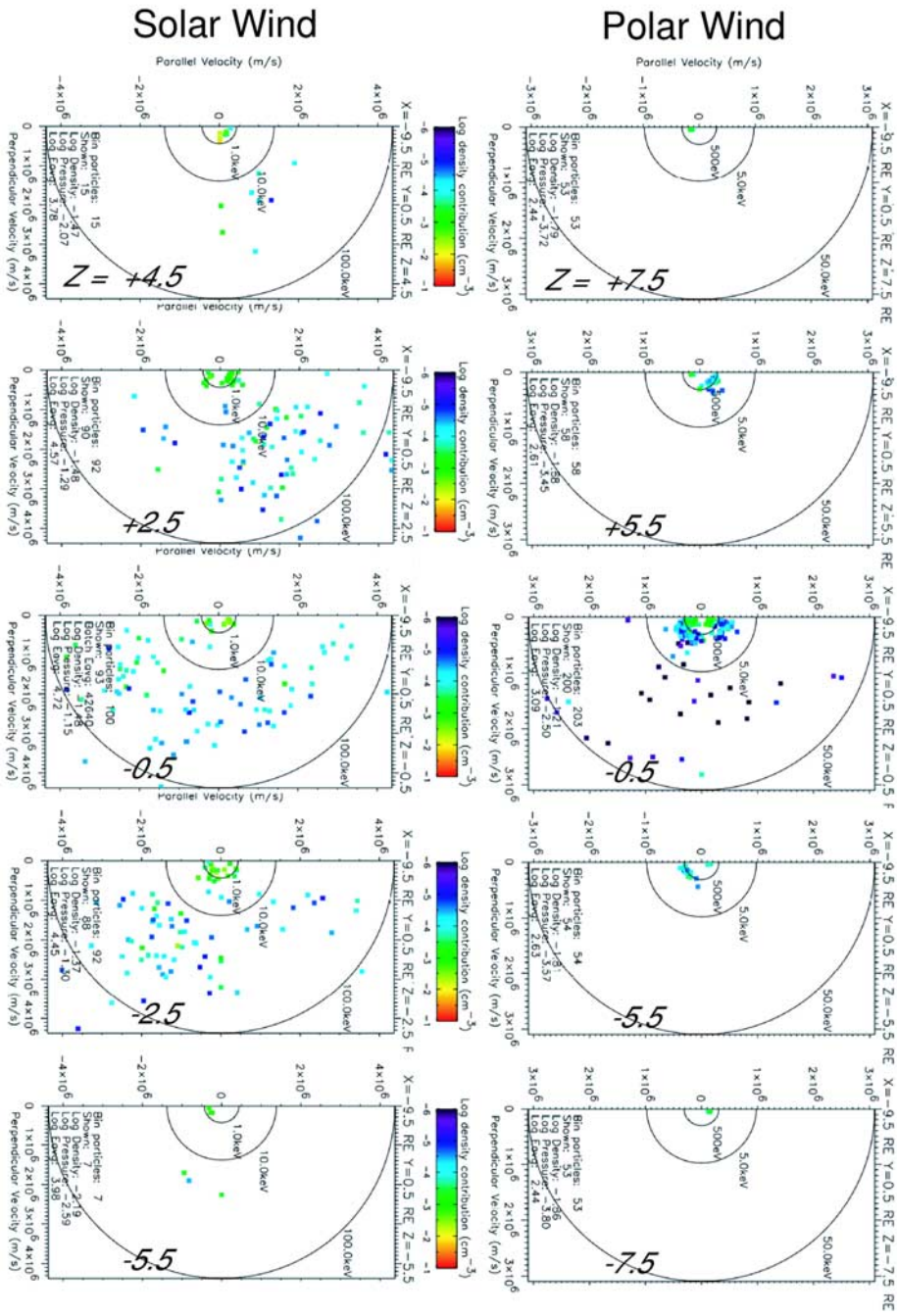

Figure 14. Velocity distributions for the SB_Z fields case at selected locations in the midnight region sampled by Polar at apogee in fall 2001 for solar wind and polar wind particles.

protons that have circulated through the inner magnetosphere, escaped into the magnetosheath and entered along the primary solar wind entry path that produces the hot solar wind component, discussed below.

[47] In the left or solar wind column, the top and bottom distributions are found at the point where the polar wind begins to counterstream, indicating closed flux tubes. In these bins we find streams of <1 keV protons traveling earthward along the local magnetic field on both northward and southward sides of the current sheet. These are the innermost mantle solar wind protons that are seen in Figure 8 to convect to the current sheet at about 30–40 R_E in the tail center. They have passed through the current sheet and are seen at this location traveling along the magnetic field in the hemisphere opposite to that from which they arrived, earthward away from the current sheet. As we move closer to the current sheet from the lobes, another solar wind proton population appears with a much higher mean energy and a much broader angular distribution. These protons have never traveled farther than about 15 R_E from Earth since their entry into the magnetosphere. They are the ones that enter direct from the dawn flank, as seen in Figure 6. Near the current sheet, this population becomes isotropic with energies between 10–100 keV; thus the solar wind

protons at this location are a mixture of hot protons that entered at dawn and traveled immediately into the ring current-like region, gaining energy from the strong convection there, with low-energy solar wind protons originating in the inner mantle flows.

[48] Figure 14 explains a number of features of the solar wind and polar wind protons in the plasma sheet. The transition from cold streaming polar wind to counterstreaming polar wind occurs at about the same location $|Z| \sim 5\ R_E$ where solar wind protons begin to stream earthward from the ''reflected'' mantle flows. The earthward solar wind streams resemble the earthward polar wind streams, since they both have been selected by the same velocity filter effect in the more distant tail. Both solar and polar winds contribute to separate warm and hot populations at this location, the hot population coming from dawn flank entry while the warm component comes from the midnight plasma sheet. The solar wind contributes more hot protons while the polar wind contributes more warm protons, in this simulation.

[49] Inner magnetospheric distributions for polar wind and solar wind protons are shown in Figure 15, at a point representative of the nonstorm ring current region just inside geosynchronous orbit near dusk. Here again, the solar protons are substantially more energetic than the polar wind protons because they have a more robust hot population while the polar wind protons have a more robust warm population. A more active period with strong flow in the midnight plasma sheet would tend to reduce the difference between the mean energies attained by solar and polar wind protons in this region. Overall, these distributions of solar wind and polar wind protons bear a striking resemblance to the distributions attributed to those sources by *Christon et al.* [1994]. The polar wind protons have a soft energy distribution that declines with energy from low to high, while the solar wind protons have a distinct peak at tens of keV. This can be seen from the energy distributions (integral over angles) shown in Figure 15.

5. Summary and Discussion

[50] We previously suggested [*Chappell et al.*, 1987; *Delcourt et al.*, 1993; *Moore and Delcourt*, 1995] that much of the plasma sheet and ring current plasma could be provided by ionospheric sources, even though it is clear that the solar wind supplies the energy to power magnetospheric phenomena. *Delcourt et al.* [1992] looked at solar wind entry and concluded that it was exceedingly difficult for solar wind protons arriving via the dayside cusp region to reach the inner magnetosphere through the plasma sheet. We failed then to consider entry along the low-latitude boundary layers near the flanks of the magnetosphere, but others have suggested or pointed out that entry path [*Lennartsson*, 1994; *Borovsky et al.*, 1997; *Richard et al.*, 2002; *Walker et al.*, 2003; *Peroomian*, 2003; *Winglee*, 2002; *Thomsen et al.*, 2003]. On the other hand, the polar wind does not seem to have been taken seriously as a source for the plasma sheet since *Hill* [1974]. Here we have taken a more comprehensive approach to solar wind entry than we did earlier, by initiating particles in the upstream solar wind and tracking them through a realistic interaction from MHD simulations. We ignored the O^+ in the magnetosphere, limiting this initial study to the light ions that supply the plasma sheet and nonstorm ring current regions. This will serve as a baseline for future studies considering the heavy ion component, originating mainly from auroral zone and cusp processes, and for study of more active periods with important dynamics.

[51] In agreement with results of others cited above, we find for SB_Z that the dawn low-latitude boundary layer region is an effective source of solar wind particles to the nonstorm ring current region. This route supplies the ring current-like region independent of another path through the midnight plasma sheet. That region is lower in solar proton density and pressure, compared with the dawn entry route, evidently because it selects the lowest-energy solar wind protons and does not heat them much for the conditions we studied. For polar wind outflows, the traditional midnight plasma sheet is the primary entry path to the inner magnetosphere, though some polar wind protons do convect out into the magnetosheath and reenter the magnetosphere along the dusk pathway taken by the majority of solar wind ions. For the SB_Z conditions we studied, the solar wind pressure contribution to the nonstorm ring current region is greater than the polar wind contribution and the two contribute comparably to density, the solar wind energy contribution having greater mean energy owing to the dawn flank entry path, which transmits thermal solar wind protons and adds substantially to their energy.

[52] Though we have not explored this here, the simulation behavior suggests that solar wind velocity may be an important parameter influencing solar wind entry into the magnetosphere via the mantle and midnight plasma sheet. Low velocity solar wind may enhance the importance of mantle entry because it contains a larger fraction of slower protons that will more successfully enter through the midnight plasma sheet. This suggests an interesting future direction for numerical experiments and correlative studies.

[53] For NB_Z conditions, solar wind entry is first through the cusp and then the flank LLBS, similarly to the SB_Z case, but not apparently favoring the dawnside. Owing to weak inner magnetospheric convection for this case, the flank LLBL source region is less effective at supplying the nonstorm ring current region, and the polar wind source becomes more important as a contribution to the weak NB_Z ring current. That the polar wind should make a stronger contribution at lower activity levels appears opposite to current expectations widely held in our community by both theorists and observers. However, those expectations are based upon O^+ participation in the ring current, which we have not considered here.

[54] Also for NB_Z conditions, a feature resembling the ''theta aurora'' phenomenon appears in this simulation, largely in solar protons entering through the cusp and then making a circuit through the dawn LLBL into the plasma sheet and back up to the high-latitude reconnection sites. It would be very interesting to look at this feature as a function of B_Y in a future study with different upstream conditions.

[55] Figure 16 summarizes our results in a concise fashion using three-dimensional cutaway diagrams. Because of the solar wind entry feature on the dawn flank, we have focused here on the dawnside of the magnetosphere.

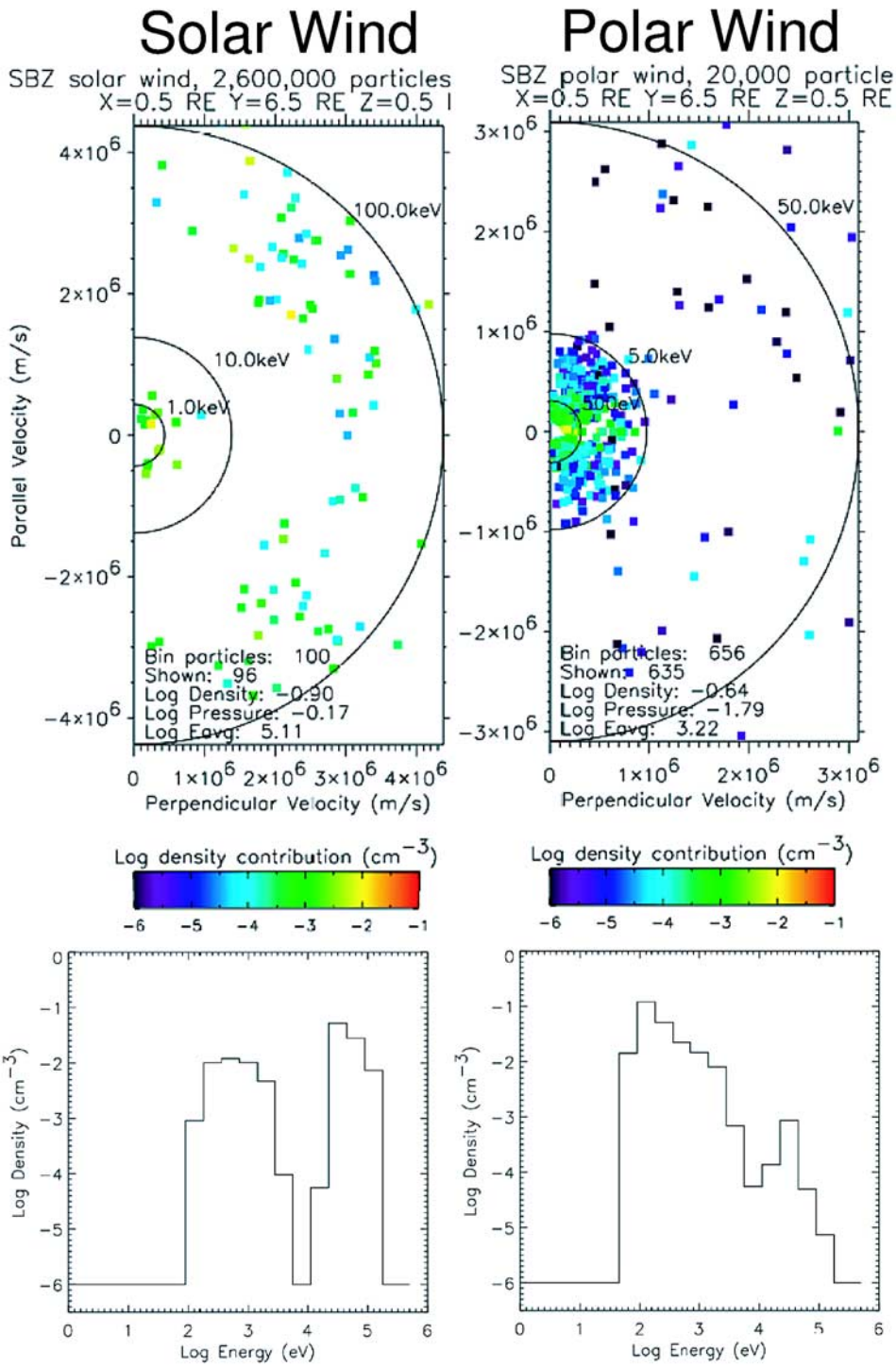

Figure 15. (top) Velocity distributions for SB_Z at indicated locations near dusk inside geosynchronous orbit for solar wind and polar wind particles. (bottom) The angle-integrated energy distribution of solar and polar wind protons.

[56] It is interesting to consider these results in the context of the geopause suggested by *Moore and Delcourt* [1995]. It is apparent that solar wind protons enjoy a special access route to the inner magnetosphere that is quite different from that taken by ionospheric outflows. Polar wind that circulates to the dayside and escapes into the magnetosheath can of course be readmitted to the magnetosphere along this same route. We interpret this route as being a result of the structure of the magnetospheric fields. It has been pointed out [*Olson and Pfitzer*, 1984; *Sibeck et al.*, 1999] that this structure leads to an entry region or channel along which solar protons from the dawn low-latitude boundary layer

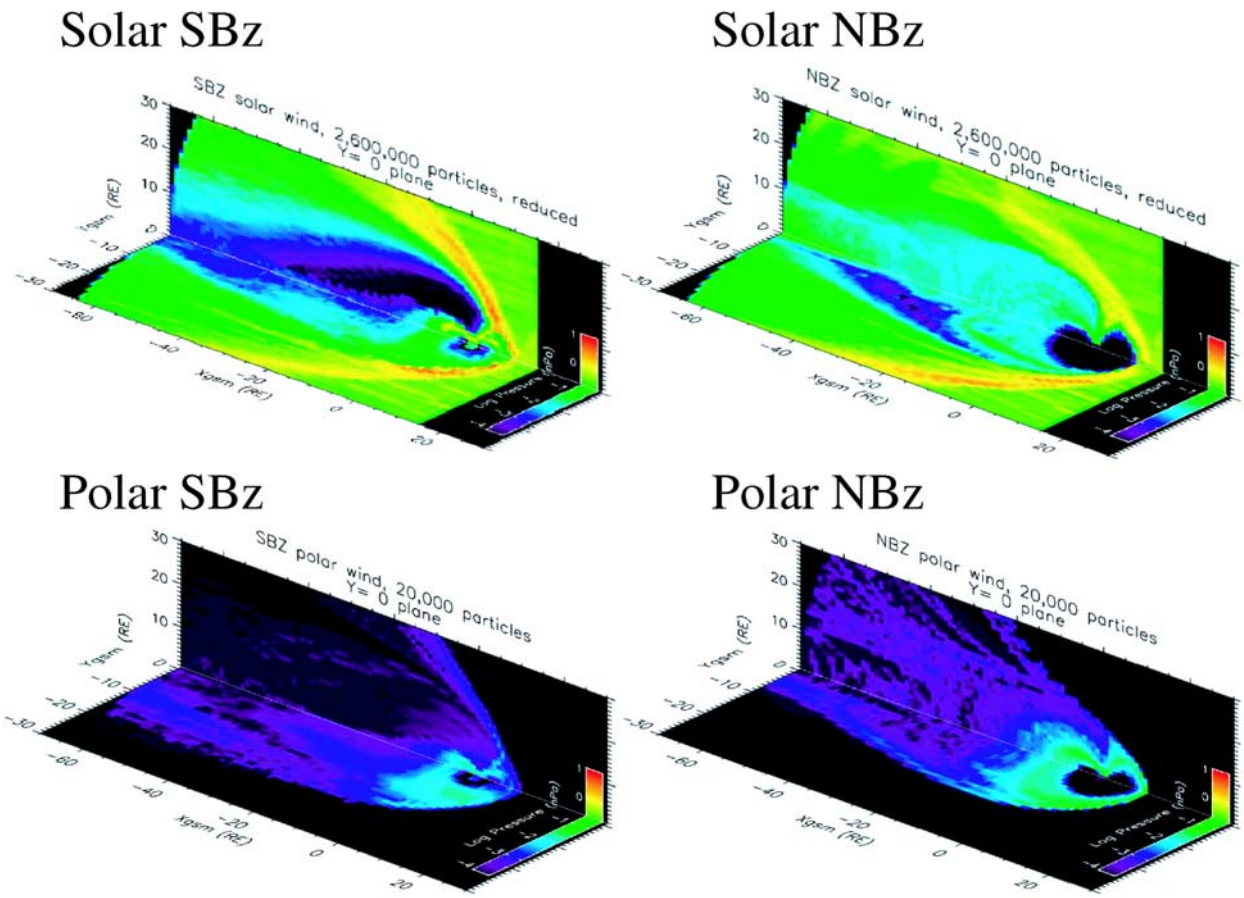

Figure 16. Summary plot showing solar and polar wind magnetospheres for SB_Z and NB_Z, with a cutaway of the pressure distribution for each corresponding case.

may enter the magnetosphere, producing considerable mixing of the two sources in the inner magnetosphere, as seen for the conditions considered here.

6. Conclusions

[57] We have investigated access to the plasma sheet and nonstorm ring current region by solar wind and polar wind plasmas using single particle trajectory calculations in fields from a global MHD simulation of SB_Z and NB_Z periods. This approach allows tracking of solar and polar wind contributions to magnetospheric plasmas. We believe this to be the first global particle simulation of polar wind circulation and kinetics within the magnetosphere. The study leads to the following main conclusions.

[58] 1. For SB_Z, we confirm other studies showing that solar wind has an important entry route along the dawn flank and convects with considerable energization into the inner magnetosphere and into the nonstorm ring current without passing through the midnight plasma sheet proper.

[59] 2. The slowest component of the solar wind also enters along the traditional route through the mantles and plasma sheet.

[60] 3. Polar wind flows substantially through the plasma sheet proper and supplies a plasma pressure contribution that is appreciable but secondary for the conditions we have studied in the geosynchronous orbit region.

[61] 4. The density contributions of solar and polar wind protons are comparable, but the solar wind protons have a substantially higher mean energy and therefore pressure.

[62] 5. For NB_Z, solar entry is via the cusps, then into the LLBL, and again entering the inner magnetosphere from along both flanks. The entering LLBL flow continues along the flank and diagonally across the plasma sheet and down tail, forming a cold dense plasma sheet. The resultant solar wind ring current is weaker and farther out from Earth than in the SB_Z case.

[63] 6. Polar wind also enters the NB_Z plasma sheet, which is distended in z and no longer shaped like a thin sheet. The polar wind bifurcates into one component that escapes downstream on reconnected field lines and another that circulates into the ring current-like region and creates a weak but appreciable pressure, earthward of the weaker ring current formed by solar wind protons.

[64] 7. Simulated velocity distribution features in the SB_Z plasma sheet agree well with Polar observations of high Mach number polar wind supply of the plasma sheet, with interpenetration of the polar wind streams from the two lobes and mantles, with heating to form counterstreaming plasma sheet boundary layer populations and a hot isotropic central plasma sheet population.

[65] 8. In the region observed by Polar, a hot solar wind proton distribution is found to occupy the current sheet region. These protons are on closed drift paths encircling the Earth for these conditions and may be considered part of the outer ring current. In the geosynchronous ring current region, the energy distributions of polar wind and solar wind protons agree well with the results from AMPTE/CCE shown by *Christon et al.* [1994] and support their identification of a soft component with mainly polar wind origins and an energetic peaked component with mainly solar wind origins.

[66] We conclude that for typical conditions of moderate activity, magnetospheric transport of polar wind and solar wind ions into the inner magnetosphere occurs along distinct paths. Solar wind enters most effectively via the dawn flank and directly into the inner plasma sheet and ring current-like regions. Polar wind enters most effectively along the traditional route through the midnight plasma sheet. As a result, the solar plasma ring current should be less affected by substorms and other magnetotail phenomena, while the polar wind or other ionospheric polar outflow contributions may be expected to depend strongly on such processes. This type of behavior has been observed recently by *Mitchell et al.* [2003], who reported strong substorm modulation of oxygen fluxes in the ring current, but with relatively little modulation of proton fluxes. We hope to return to this issue with a further study of auroral O^+ outflow behavior in the same fields we have used here to study polar wind protons.

[67] **Acknowledgments.** We are indebted to Manuel Buenfil for extensive creative computational and visualization support of this investigation. The authors acknowledge support from the GSFC Polar Mission under UPN 370-08 for TIDE and TIMAS data analysis and from the NASA Geospace Sciences Program under UPN 344-42-01 for the Terrestrial Plasma Energization investigation.

[68] Lou-Chuang Lee thanks Vahe Peroomian and another reviewer for their assistance in evaluating this paper.

References

Baker, D. N., R. E. Ergun, J. L. Burch, J.-M. Jahn, P. W. Daly, R. Friedel, G. D. Reeves, T. A. Fritz, and D. G. Mitchell (2002), A telescopic and microscopic view of a magnetospheric substorm on 31 March 2001, *Geophys. Res. Lett*, *29*(18), 1862, doi:10.1029/2001GL014491.

Banks, P. M., and T. E. Holzer (1969), Features of high latitude plasma transport in the upper atmosphere, *J. Geophys. Res.*, *74*, 6304.

Borovsky, J. E., M. F. Thomsen, and D. J. McComas (1997), The superdense plasma sheet: Plasmaspheric origin, solar wind origin, or ionospheric origin?, *J. Geophys. Res.*, *102*(A10), 22,089.

Cattell, C. A., J. Dombeck, J. R. Wygant, M. K. Hudson, F. S. Mozer, M. A. Temerin, W. K. Peterson, C. A. Kletzing, C. T. Russell, and R. F. Pfaff (1999), Comparisons of Polar satellite observations of solitary wave velocities in the plasma sheet boundary and the high altitude cusp to those in the auroral zone, *Geophys. Res. Lett.*, *26*(3), 425.

Chandler, M. O., and T. E. Moore (2003), Observations of the geopause at the equatorial magnetopause: Density and temperature, *Geophys. Res. Lett.*, *30*(16), 1869, doi:10.1029/2003GL017611.

Chappell, C. R., T. E. Moore, and J. H. Waite Jr. (1987), The ionosphere as a fully adequate source of plasma for the Earth's magnetosphere, *J. Geophys. Res.*, *92*, 5896.

Chen, S.-H., and T. E. Moore (2004), Dayside flow bursts in the Earth's magnetosphere, *J. Geophys. Res.*, *109*, A03215, doi:10.1029/2003JA010007.

Christon, S. P., G. Gloeckler, D. C. Hamilton, and F. M. Ipavich (1994), A method for estimating the solar wind H^+ contribution to magnetospheric plasma, in *Solar Terrestrial Energy Program, 5th COSPAR Colloquium*, edited by D. N. Baker, V. O. Patitashvili and M. J. Teague, Elsevier, New York.

Cully, C. M., E. F. Donovan, A. W. Yau, and H. J. Opgenoorth (2003), Supply of thermal ionospheric ions to the central plasma sheet, *J. Geophys. Res*, *108*(A2), 1092, doi:10.1029/2002JA009457.

Daglis, I. A., G. Kasotakis, E. T. Sarris, Y. Kamide, S. Livi, and B. Wilken (1999), Variations in the ion composition during an intense magnetic storm and their consequences, *Phys. Chem. Earth*, *24*, 229.

Delcourt, D. C., C. R. Chappell, T. E. Moore, and J. H. Waite Jr. (1989), A three-dimensional numerical model of ionospheric plasma in the magnetosphere, *J. Geophys. Res.*, *94*, 11,893.

Delcourt, D. C., T. E. Moore, J. A. Sauvaud, and C. R. Chappell (1992), Nonadiabatic transport features in the outer cusp region, *J. Geophys. Res.*, *97*(A11), 16,833.

Delcourt, D. C., J. A. Sauvaud, and T. E. Moore (1993), Polar wind dynamics in the magnetotail, *J. Geophys. Res.*, *98*(A6), 9155.

Delcourt, D. C., T. E. Moore, and C. R. Chappell (1994), Contributions of low-energy ionospheric protons to the plasma sheet, *J. Geophys. Res.*, *99*(A4), 5681.

Eastman, T. E., L. A. Frank, W. K. Peterson, and W. Lennartsson (1984), The plasma sheet boundary layer, *J. Geophys. Res.*, *89*, 1553.

Elphic, R. C., M. F. Thomsen, and J. E. Borovsky (1997), The fate of the outer plasmasphere, *Geophys. Res. Lett.*, *24*, 365.

Fedder, J. A., J. G. Lyon, S. P. Slinker, and C. M. Mobarry (1995), Topological structure of the magnetotail as a function of interplanetary magnetic field direction, *J. Geophys. Res.*, *100*, 3613.

Freeman, J. W., Jr., H. K. Hills, T. W. Hill, P. H. Reiff, and D. A. Hardy (1977), Heavy ion circulation in the Earth's magnetosphere, *Geophys. Res. Lett.*, *4*, 195.

Goldstein, J., R. W. Spiro, P. H. Reiff, R. A. Wolf, B. R. Sandel, J. W. Freeman, and R. L. Lambour (2002), IMF-driven overshielding electric field and the origin of the plasmaspheric shoulder of May 24, 2000, *Geophys. Res. Lett.*, *29*(16), 1819, doi:10.1029/2001GL014534.

Grebowsky, J. M. (1970), Model study of plasmapause motion, *J. Geophys. Res.*, *75*, 4329.

Hamilton, D. C., G. Gloecker, F. M. Ipavich, W. Studemann, B. Wilken, and G. Kremser (1988), Ring current development during the great geomagnetic storm of February, 1986, *J. Geophys. Res.*, *93*, 14,343.

Hill, T. W. (1974), Origin of the plasma sheet, *Rev. Geophys.*, *12*, 379.

Kletzing, C. A., and J. D. Scudder (1999), Auroral-plasma sheet electron anisotropy, *Geophys. Res. Lett.*, *26*(7), 971.

Klumpar, D. M. (1979), Transversely accelerated ions: An ionospheric source of hot magnetospheric ions, *J. Geophys. Res.*, *84*, 4229.

Lennartsson, W. (1994), Tail lobe ion composition at energies of 0.1 to 16keV/e: Evidence for mass-dependent density gradients, *J. Geophys. Res.*, *99*(A2), 2387.

Mitchell, D. G., P. C. Brandt, E. C. Roelof, D. C. Hamilton, K. C. Retterer, and S. Mende (2003), Global imaging of O^+ from IMAGE/HENA, *Space Sci. Rev.*, *109*, 63.

Mobarry, C. M., J. A. Fedder, and J. G. Lyon (1996), Equatorial plasma convection from global simulations of the Earth's magnetosphere, *J. Geophys. Res.*, *101*, 7859.

Moore, T. E., and D. C. Delcourt (1995), The geopause, *Rev. Geophys*, *33*(2), 175.

Moore, T. E., et al. (1995), The thermal ion dynamics experiment and plasma source instrument, *Space Sci. Rev.*, *71*, 409.

Moore, T. E., et al. (1997), High-altitude observations of the polar wind, *Science*, *277*, 349.

Moore, T. E., et al. (1999), Source processes in the high latitude ionosphere, *Space Sci. Rev.*, *88*(1–2), 7.

Moore, T. E., B. L. Giles, D. C. Delcourt, and M.-C. Fok (2000), The plasma sheet source groove, *J. Atmos. Solar Terr. Phys.*, *62*(6), 505.

Nakamura, R., et al. (2002), Fast flow during current sheet thinning, *Geophys. Res. Lett.*, *29*(23), 2140, doi:10.1029/2002GL016200.

Olson, W. P., and K. A. Pfitzer (1984), The entry of AMPTE lithium ions into a magnetically closed magnetosphere, *J. Geophys. Res.*, *89*, 7347.

Parks, G., L. J. Chen, M. McCarthy, D. Larson, R. P. Lin, T. Phan, H. Reme, and T. Sanderson (1998), New observations of ion beams in the plasma sheet boundary layer, *Geophys. Res. Lett.*, *25*(17), 3285.

Peroomian, V. (2003), The influence of the interplanetary magnetic field on the entry of solar wind ions into the magnetosphere, *Geophys. Res. Lett.*, *30*(7), 1407, doi:10.1029/2002GL016627.

Peterson, W. K., R. D. Sharp, E. G. Shelley, R. G. Johnson, and H. Balsiger (1981), Energetic ion composition of the plasma sheet, *J. Geophys. Res.*, *86*, 761.

Peterson, W. K., E. G. Shelley, G. Haerendel, and G. Paschmann (1982), Energetic ion composition in the subsolar magnetopause and boundary layer, *J. Geophys. Res.*, *87*, 2139.

Richard, R. L., M. El-Alaoui, M. Ashour-Abdalla, and R. J. Walker (2002), Interplanetary magnetic field control of the entry of solar energetic particles into the magnetosphere, *J. Geophys. Res.*, *107*(A8), 1184, doi:10.1029/2001JA000099.

Sandel, B. R., et al. (2001), Initial results from the IMAGE extreme ultraviolet imager, *Geophys. Res. Lett.*, *28*(8), 1439.

Sharp, R. D., R. G. Johnson, and E. G. Shelley (1977), Observation of an ionospheric acceleration mechanism producing energetic (keV) ions primarily normal to the geomagnetic field direction, *J. Geophys. Res.*, *82*(22), 3324.

Sharp, R. D., W. Lennartsson, and R. J. Strangeway (1985), The ionospheric contribution to the plasma environment in near-earth space, *Radio Sci.*, *20*, 456.

Shelley, E. G., R. G. Johnson, and R. D. Sharp (1972), Satellite observations of energetic heavy ions during a geomagnetic storm, *J. Geophys. Res.*, *77*, 6104.

Sibeck, D. G., et al. (1999), Plasma transfer processes at the magnetopause, *Space Sci. Rev.*, *88*(1–2), 207.

Slinker, S. P., J. A. Fedder, and J. G. Lyon (1995), Plasmoid formation and evolution in a numerical simulation of a substorm, *Geophys. Res. Lett.*, *22*(7), 859.

Slinker, S. P., J. A. Fedder, J. Chen, and J. G. Lyon (1998), Global MHD simulation of the magnetosphere and ionosphere for 1930–2330 UT on November 3, 1993, *J. Geophys. Res.*, *103*, 26,243.

Slinker, S. P., J. A. Fedder, J. M. Ruohoniemi, and J. G. Lyon (2001), Global MHD simulation of the magnetosphere for November 24, 1996, *J. Geophys. Res.*, *106*, 361.

Stern, D. P. (1975), The motion of a proton in the equatorial magnetosphere, *J. Geophys. Res.*, *80*, 595.

Su, Y.-J., J. L. Horwitz, T. E. Moore, M. O. Chandler, P. D. Craven, B. L. Giles, M. Hirahara, and C. J. Pollock (1998), Polar wind survey with Thermal Ion Dynamics Experiment/Plasma Source Instrument suite aboard POLAR, *J. Geophys. Res.*, *103*, 29,305.

Su, Y.-J., J. E. Borovsky, M. F. Thomsen, N. Dubouloz, M. O. Chandler, T. E. Moore, and M. Bouhram (2001), Plasmaspheric material on high-latitude open field lines, *J. Geophys. Res.*, *106*, 6085.

Thomsen, M. F., J. E. Borovsky, R. M. Skoug, and C. W. Smith (2003), The delivery of cold, dense plasma sheet material into the near-earth region, *J. Geophys. Res.*, *108*(A4), 1151, doi:10.1029/2002JA009544.

Tsyganenko, N. A. (1989), A magnetospheric magnetic field model with a warped tail current sheet, *Planet. Space Sci.*, *37*, 5.

Volland, H. (1978), A model of the magnetospheric convection electric field, *J. Geophys. Res.*, *83*, 2695.

Walker, R. J., M. Ashour-Abdalla, T. Ogino, V. Peroomian, and R. L. Richard (2003), Modeling magnetospheric sources, in *Earth's Low-Latitude Boundary Layer*, *Geophys. Monogr. Ser.*, vol. 133, edited by P. Newell and T. Onsager, p. 33, AGU, Washington, D. C.

Winglee, R. M. (2002), Circulation of ionospheric and solar wind particle populations during extended southward interplanetary magnetic field, *J. Geophys. Res.*, *108*(A10), 1385, doi:10.1029/2002JA009819.

M. O. Chandler, National Space Science and Technology Center, NASA Marshall Space Flight Center, Mail Code SD50, Huntsville, AL 35899, USA.

C. R. Chappell and M. Huddleston, Vanderbilt University, Nashville, TN 37203, USA.

S. P. Christon, M.-C. Fok, and T. E. Moore, NASA Goddard Space Flight Center, Mail Code 612.2, Greenbelt, MD 20771, USA. (thomas.e.moore@gsfc.nasa.gov)

D. C. Delcourt, Centre d'Etude des Environnements Terrestre et Planétaires, 4 Ave. de Neptune, St. Maur, F-94017 France.

J. Fedder, George Mason University, 4400 University Drive, Vienna, VA 22030, USA.

M. Liemohn, University of Michigan, 2455 Hayward Street, Ann Arbor, MI 48109, USA.

W. K. Peterson, University of Colorado, 1234 Innovation Drive, Boulder, CO 80303, USA.

S. Slinker, Naval Research Laboratory, 4555 Overlook Avenue, SW, Washington, DC 20375, USA.